

---

# OoD-Bench: Benchmarking and Understanding Out-of-Distribution Generalization Datasets and Algorithms

---

Nanyang Ye<sup>1\*</sup>, Kaican Li<sup>2\*</sup>, Lanqing Hong<sup>2</sup>, Haoyue Bai<sup>3</sup>, Yiting Chen<sup>1</sup>,  
Fengwei Zhou<sup>2</sup>, Zhenguo Li<sup>2</sup>

<sup>1</sup> Shanghai Jiao Tong University, <sup>2</sup> Huawei Noah's Ark Lab,

<sup>3</sup> The Hong Kong University of Science and Technology

## Abstract

Deep learning has achieved tremendous success with independent and identically distributed (i.i.d.) data. However, the performance of neural networks often degenerates drastically when encountering out-of-distribution (OoD) data, i.e., training and test data are sampled from different distributions. While a plethora of algorithms has been proposed to deal with OoD generalization, our understanding of the data used to train and evaluate these algorithms remains stagnant. In this work, we position existing datasets and algorithms from various research areas (e.g., domain generalization, stable learning, invariant risk minimization) seemingly unconnected into the same coherent picture. First, we identify and measure two distinct kinds of distribution shifts that are ubiquitous in various datasets. Next, we compare various OoD generalization algorithms with a new benchmark dominated by the two distribution shifts. Through extensive experiments, we show that existing OoD algorithms that outperform empirical risk minimization on one distribution shift usually have limitations on the other distribution shift. The new benchmark may serve as a strong foothold that can be resorted to by future OoD generalization research.

## 1 Introduction

Deep learning has been widely adopted in various applications of computer vision [28] and natural language processing [22] with great success, under the implicit assumption that the training and test data are drawn independent and identically distributed (i.i.d.) from the same distribution. While neural networks often exhibit super-human generalization performance on the training distribution, they can be susceptible to minute changes in the test distribution [57, 66]. This is problematic because sometimes true underlying data distributions are significantly underrepresented or misrepresented by the limited training data at hand. In the real world, such mismatches are commonly observed [35, 25], and have led to significant performance drops in many deep learning algorithms [e.g., 9, 37, 46]. As a result, the reliability of current learning systems is substantially undermined in critical applications such as medical imaging [18, 4], autonomous driving [20, 70, 6, 63], and security systems [33].

*Out-of-Distribution (OoD) Generalization*, the task of generalizing under such distribution shifts, is traditionally known as Domain Generalization (DG) in deep learning. The setting of OoD generalization (or DG)<sup>2</sup> assumes access to multiple datasets during training, each of them containing examples about the same task, but collected under a different environment or experimental condition [14, 47].

---

\*These authors contributed equally.

<sup>2</sup>In the rest of this paper, we make no distinction between OoD generalization and DG (or between *environments* and *domains*), but the former is preferred for a greater audience.

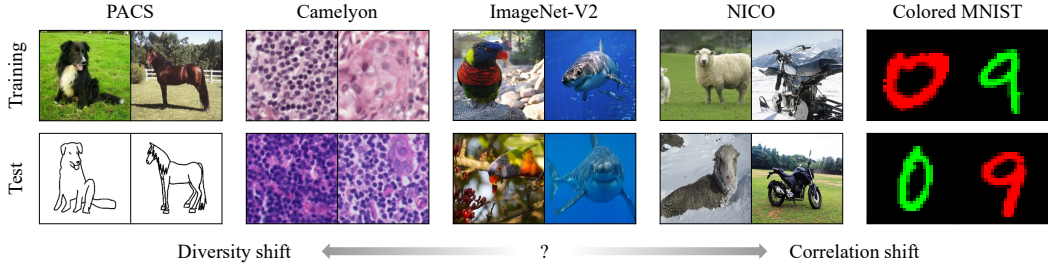


Figure 1: Examples of image classification datasets demonstrating different kinds of distribution shifts. While it is clear that the datasets at both ends exhibit apparent distribution shifts, in the middle, it is hard to distinguish the differences in distribution between the training dataset (ImageNet [21]) and the test dataset (ImageNet-V2 [58]), which represent a large body of realistic OoD datasets.

The goal of OoD generalization algorithms is to incorporate the invariance across these training environments into a classifier, in hopes that such invariance will also hold in unseen test environments [27]. Driven by this motivation, numerous algorithms have been proposed over the years [81], each claimed to have surpassed all its precedents on a particular genre of benchmark. However, a recent work by Gulrajani and Lopez-Paz [27] suggests that our current progress might have been overestimated—most of the advanced learning algorithms tailor-made for OoD generalization are still on par with the classic Empirical Risk Minimization (ERM) [68].

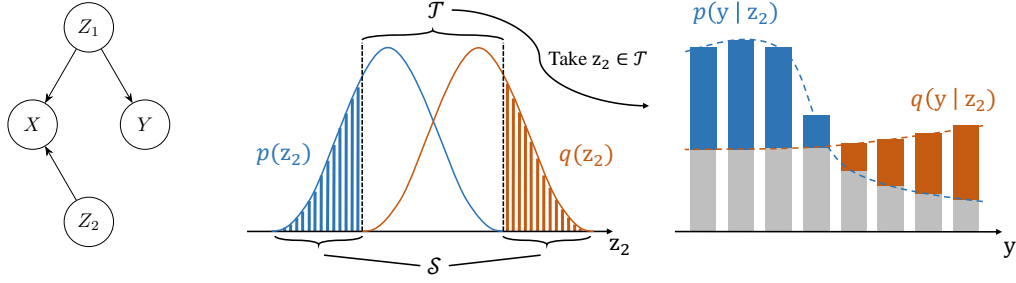
In this work, we validate the effectiveness of some OoD generalization algorithms and reveal a possible reason as to why they appear to be no much better than ERM, which is unexplained in DomainBed [27]. As it turns out, incumbent datasets exhibiting distribution shifts can be generally divided into two categories of different characteristics. The majority of the algorithms have only surpassed ERM in at most one of the categories. **We hypothesize that the phenomenon is due to the influence of two distinct kinds of distribution shift, namely *diversity shift* and *correlation shift*, while preexisting literature often focuses on merely one of them.**

Normally, datasets such as VLCS [67], PACS [39], Office-Home [69], and DomainNet [54] that consist of multiple domains are used to train and evaluate DG models. In these datasets, each domain represents a certain spectrum of diversity in data. During experiments, these domains are further grouped into training and test domains, leading to the diversity shift. Although extensive research efforts have been dedicated to the datasets dominated by diversity shift, it is not until recently that Arjovsky et al. [7] draws attention to another challenging generalization problem stemmed from spurious correlations. Colored MNIST, a variant of MNIST [38], is constructed by coloring the digits with either red or green to highlight the problem. The colored digits are arranged into training and test environments such that the labels and colors are strongly correlated, but the correlation relationship flips across the environments, creating the correlation shift.

As shown in Figure 1, diversity and correlation shift are of clearly different nature. At the extremes, discrepancies between training and test environments become so apparent that great troubles are often caused for algorithms trying to generalize [39, 7]. Interestingly, in some real-world cases such as ImageNet versus ImageNet-V2 where the discrepancy is virtually imperceptible, neural networks are still unable to generalize satisfactorily, of which the reason is not fully understood [57]. In Figure 3, our estimation of diversity and correlation shift shed some light on the issue—there is a non-trivial degree of correlation shift between the original ImageNet and the variant. Besides, other OoD datasets have also shown varying degrees of diversity and correlation shift. Based on the findings and analysis in this work, we make three recommendations for future OoD generalization research:

- Evaluate OoD generalization algorithms comprehensively on two types of datasets, one dominated by diversity shift and the other dominated by correlation shift. These two distribution shifts can be measured by our method (as described in the next section).
- Investigate the nature of distribution shift in OoD problems before designing algorithms as the optimal treatment for different kinds of distribution shift may be different.
- Design large-scale datasets that more subtly capture real-world distribution shifts as imperceptible distribution shifts can also be conspicuous to neural networks shown by our analysis.

## 2 OoD-Bench: Diversity Shift and Correlation Shift



(a) Causal graph depicting the causal influence among the concerned variables. (b) Illustration of diversity shift and correlation shift. Diversity shift amounts to half of the summed area of the colored regions in the left figure. Correlation shift is an integral over  $\mathcal{T}$ , where every integrand can be seen as the summed heights of the colored bars in the right figure then weighted by the square root of  $p(\mathbf{z}_2) \cdot q(\mathbf{z}_2)$ .

Figure 2: Explanatory illustrations for diversity and correlation shift.

In the setting of supervised learning, every input  $\mathbf{x} \in \mathcal{X}$  is assigned with a label  $\mathbf{y} \in \mathcal{Y}$  by some fixed labeling rule  $f: \mathcal{X} \rightarrow \mathcal{Y}$ . The inner mechanism of  $f$  usually depends on a particular set of features  $\mathcal{Z}_1$ , whereas the rest of the features  $\mathcal{Z}_2$  are not causal to prediction. For example, we assign the label “airplane” to the image of an airplane regardless of its color or whether it is landed or flying. The causal graph in Figure 2a succinctly depicts the interplay among the underlying random variables of our model: the input variable  $X$  is determined by the latent variables  $Z_1$  and  $Z_2$ , whereas the target variable  $Y$  is determined by  $Z_1$  alone. Similar graphs can be found in [2, Fig. 1a] and [44, Fig. 1].

For every labeled dataset, consider its training environment  $\mathcal{E}_{\text{tr}}$  and test environment  $\mathcal{E}_{\text{te}}$  to be distributions over  $\mathcal{X} \times \mathcal{Y} \times \mathcal{Z}$  where  $\mathcal{Z} = \mathcal{Z}_1 \times \mathcal{Z}_2$ . Moreover,  $\mathcal{E}_{\text{tr}}$  and  $\mathcal{E}_{\text{te}}$  are associated with two non-negative probability functions  $p$  and  $q$ . For ease of exposition, we assume no label shift [8] across the environments, which means that  $p_Y(\mathbf{y}) = q_Y(\mathbf{y})$  for every  $\mathbf{y} \in \mathcal{Y}$ . In a valid OoD generalization problem,  $\mathcal{E}_{\text{tr}}$  and  $\mathcal{E}_{\text{te}}$  must share the same labeling rule  $f$ . To put it in the language of causality [53], the *direct cause* of  $Y$  (which is  $Z_1$ ) must be observable in both environments and the causal mechanism that  $Z_1$  exerts on  $Y$  must be constant at all times. Formally, it dictates that

$$p_{Z_1}(\mathbf{z}_1) \cdot q_{Z_1}(\mathbf{z}_1) \neq 0 \wedge \forall \mathbf{y} \in \mathcal{Y} : p_{Y|Z_1}(\mathbf{y} | \mathbf{z}_1) = q_{Y|Z_1}(\mathbf{y} | \mathbf{z}_1) \quad (1)$$

for every  $\mathbf{z}_1 \in \mathcal{Z}_1$ . Hence, there exists an algorithm that can achieve equally good performance in both  $\mathcal{E}_{\text{tr}}$  and  $\mathcal{E}_{\text{te}}$ , which makes OoD generalization possible. On the contrary, the presence of  $\mathbf{z}_2 \in \mathcal{Z}_2$  satisfying

$$p_{Z_2}(\mathbf{z}_2) \cdot q_{Z_2}(\mathbf{z}_2) = 0 \vee \exists \mathbf{y} \in \mathcal{Y} : p_{Y|Z_2}(\mathbf{y} | \mathbf{z}_2) \neq q_{Y|Z_2}(\mathbf{y} | \mathbf{z}_2) \quad (2)$$

makes OoD generalization challenging. Now we are now just one step away from our mathematical definition for diversity and correlation shift. For conciseness, we omit the subscripted random variables when referring to probability functions, e.g.,  $p_{Y|Z_2}(\mathbf{y} | \mathbf{z}_2)$  will become  $p(\mathbf{y} | \mathbf{z}_2)$ . Based on condition (2), we partition  $\mathcal{Z}_2 \subset \mathbb{R}^n$  into two (disjoint) subspaces

$$\mathcal{S} = \{\mathbf{z}_2 \in \mathcal{Z}_2 \mid p(\mathbf{z}_2) q(\mathbf{z}_2) = 0\} \quad \text{and} \quad \mathcal{T} = \{\mathbf{z}_2 \in \mathcal{Z}_2 \mid p(\mathbf{z}_2) q(\mathbf{z}_2) \neq 0\}, \quad (3)$$

which then defines diversity and correlation shift:

$$d_{\text{div}}(p, q) = \frac{1}{2} \int_{\mathcal{S}} |p(\mathbf{z}_2) - q(\mathbf{z}_2)| d^n \mathbf{z}_2, \quad (4)$$

$$d_{\text{cor}}(p, q) = \frac{1}{2} \int_{\mathcal{T}} \sqrt{p(\mathbf{z}_2) q(\mathbf{z}_2)} \sum_{\mathbf{y} \in \mathcal{Y}} |p(\mathbf{y} | \mathbf{z}_2) - q(\mathbf{y} | \mathbf{z}_2)| d^n \mathbf{z}_2, \quad (5)$$

where we assume  $\mathcal{Y}$  to be discrete. Figure 2b illustrates the definitions above when  $n = 1$ . It can be proved that the values of  $d_{\text{div}}$  and  $d_{\text{cor}}$  are bounded in  $[0, 1]$  (see Appendix A). In particular, the square root in (5) serves as a coefficient regulating the integrand because features that hardly appear in either environment should have a small contribution to the correlation shift overall. The appearance

of square roots over products of two probability functions is not new in distance metrics, as can be found in the Hellinger distance [30].

Nevertheless, we are aware that these are not the only viable formulations, yet they produce intuitively reasonable and numerically stable results even when estimated by a simple method described next. Our characterization of diversity and correlation shift provides a formal way to measure the main difficulties that hinder learning machines from generalizing out-of-distribution.

**Practical estimation** To compute diversity and correlation shift as in (4) and (5), a feature extractor that maps  $\mathcal{X}$  to  $\mathcal{Z}_2$  must be learned first. In practice, we train a simple neural network to extract these features. The network consists of a feature extractor and a linear classifier that will be discarded after training. During training, instead of predicting  $y$  given  $x$ , the network tries to predict the environment from which  $x$  is sampled, with  $y$  provided as an additional input. Hence, the feature extractor learns to extract features with varying distribution across the environments and ignores the ones that are invariant. It can be proved that  $\mathcal{Z}_2$  are represented by these features. After acquiring the essential features, we apply Kernel Density Estimation (KDE) [59, 52] to estimate the values of  $p$  and  $q$ . The integrals are then approximated by Monte Carlo Integration under importance sampling [50]. See Appendix B for more theoretical justifications on our method and pseudo codes of the whole procedure.

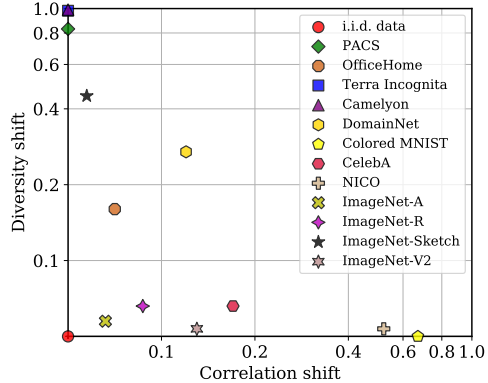


Figure 3: Estimation of diversity and correlation shift in various datasets. For ImageNet variants, the estimates are computed with respect to the original ImageNet. Log-scaled for better visualization. See Appendix C for the results in numeric form.

The results in Figure 3 which align with our intuition are obtained by the aforementioned method. Most of the existing OoD benchmarks lie over or near the axes, dominated by one kind of shift. For datasets under unknown distribution shift such as ImageNet-A [31], ImageNet-R [32], and ImageNet-V2, our method successfully decomposes the shift into the two dimensions of diversity and correlation, and therefore one may choose the appropriate algorithms based on the estimation. As shown by our benchmark results in the next section, such choices might be crucial as most OoD generalization algorithms do not perform equally well on two groups of datasets, one dominated by diversity shift and the other dominated by correlation shift.

### 3 Experiment

Previously, we have numerically positioned OoD datasets using OoD-Bench. In this section, we run algorithms on these datasets to reveal the two-dimensional trend for existing datasets and algorithms. All experiments are conducted on Pytorch 1.4 with Tesla V100 GPUs. More implementation details can be found in the Appendix.

#### 3.1 Benchmark

**Datasets** In our experiment, datasets are chosen to cover as much variety from different OoD research areas as possible. As mentioned earlier, the datasets demonstrated two-dimensional properties shown by their estimated diversity and correlation shift. The following datasets are dominated by diversity shift:

- **PACS** [39] and **OfficeHome** [69] are common DG benchmarks. These datasets contain images of objects and creatures depicted in different styles such as clipart and sketch.
- **Terra Incognita** [12] contains photographs of wild animals taken by camera traps at different locations in nature, simulating a real-world scenario for OoD generalization.
- **WILDS-Camelyon17** [35] contains histopathological image slides collected and processed by different hospitals. Data variation among these hospitals arises from sources like differences in the patient population or in slide staining and image acquisition.

On the other hand, these datasets are dominated by correlation shift:

- **Colored MNIST** [7] is a variant of the MNIST handwritten digit classification dataset [38]. Environment  $e \in \{0.1, 0.2, 0.9\}$  contains a disjoint set of digits colored either red or green. The label is a noisy function of the digit and color, such that color bears correlation  $d$  with the label and the digit bears correlation 0.75 with the label.
- **NICO** [29] consists of real-world photos of animals and vehicles captured in a wide range of contexts such as “in water”, “on snow” and “flying”. Our version of this dataset simulates a scenario where animals and vehicles are spuriously correlated with different contexts.
- **CelebA** [45] is a large-scale face attributes dataset. It has been widely used in AI fairness studies [56, 74, 19] as well as OoD generalization research [62, 55]. Similar to the setting proposed by Sagawa et al. [62], our version treats “hair color” as the target and “gender” as the spurious attribute.

For PACS, OfficeHome, and Terra Incognita, we adopt the leave-one-domain-out evaluation scheme following [27]. We train multiple models in every run with each treating one of the domains as the test environment and the rest of the domains as the training environments. The final accuracy is the mean accuracy over all such splits. For other datasets, the training and test environments are fixed, as the leave-one-domain-out scheme would render the settings of Colored MNIST, etc., much less meaningful. For more details about dataset statistics and environment splits, see Appendix D.

**Algorithms** We have selected Empirical Risk Minimization [ERM 68] and several representative algorithms from different OoD research areas for our benchmark: Group Distributionally Robust Optimization [GroupDRO 62], Inter-domain Mixup [Mixup 75, 76], Meta-Learning for Domain Generalization [MLDG 40], Domain-Adversarial Neural Networks [DANN 24], Deep CORrelation ALignment [CORAL 64], Maximum Mean Discrepancy [MMD 41], Invariant Risk Minimization [IRM 7], Variance Risk Extrapolation [VREx 37], Adaptive Risk Minimization [ARM 78], Marginal Transfer Learning [MTL 15], Style-Agnostic Networks [SagNet 49], Representation Self Challenging [RSC 34], Learning Explanations that are Hard to Vary [ANDMask 51], Out-of-Distribution Generalization with Maximal Invariant Predictor [IGA 36], and Entropy Regularization for Domain Generalization [ERDG 79].

**Implementation choices** As there is still no consensus on what model selection methods should be used in OoD generalization research [27], appropriate selection methods are chosen for each dataset in our study. To be consistent with existing lines of work [39, 17, 49, 34, 37], models trained on PACS and OfficeHome are selected by *training-domain validation*, and so is for Terra Incognita. As for WILDS-Camelyon and NICO, *OoD validation* method is adopted in respect of [35] and [10]. The two remaining datasets, Colored MNIST and CelebA, use *test-domain validation* which has been seen in [7, 37, 1, 55]. As a side note, it may be improper to apply training-domain validation to datasets dominated by correlation shift since under the influence of spurious correlations, achieving excessively high accuracy in the training environments often leads to low accuracy in novel test environments. The definitions of these model selection methods are provided in Appendix F.

Unlike DomainBed, we use a simpler model, ResNet-18 [28], for all algorithms and datasets excluding Colored MNIST, for it is the common practice in previous works [34, 49, 79, 23, 17]. Moreover, we believe smaller models could enlarge the gaps in OoD generalization performance among all the algorithms, as larger models are generally more robust to OoD data [32] and thus the performance is easier to saturate on small datasets. The ResNet-18 is pretrained on ImageNet and then finetuned on any given dataset with only one exception—NICO, which contains photos of animals and vehicles largely overlapped with ImageNet classes. For simplicity, we continue to use a two-layer perceptron following [7, 37, 55] on Colored MNIST.

**Hyperparameter search** For a fair comparison, we adopt the following hyperparameter search protocol: a 20-times random search is conducted for every pair of dataset and algorithm, and then the search process is repeated for another two random series of hyperparameter combinations, weight initializations, and dataset splits. Altogether, the three series yield the three best accuracies over which a mean and standard error bar is computed for every dataset-algorithm pair. See Appendix G for the hyperparameter search space for individual algorithms.

Table 1: Performance of ERM and OoD generalization algorithms on datasets *dominated by diversity shift*. Every symbol  $\downarrow$  denotes a score of -1, and every symbol  $\uparrow$  denotes a score of +1; otherwise the score is 0. Adding up the scores across all datasets produces the ranking score for each algorithm.

| Algorithm       | PACS                      | OfficeHome                | TerraInc                  | Camelyon                  | Average | Ranking score |
|-----------------|---------------------------|---------------------------|---------------------------|---------------------------|---------|---------------|
| RSC [34]        | $82.8 \pm 0.4^\uparrow$   | $62.9 \pm 0.4^\downarrow$ | $43.6 \pm 0.5^\uparrow$   | $94.9 \pm 0.2^\uparrow$   | 71.1    | +2            |
| MMD [41]        | $81.7 \pm 0.2^\uparrow$   | $63.8 \pm 0.1^\uparrow$   | $38.3 \pm 0.4^\downarrow$ | $94.9 \pm 0.4^\uparrow$   | 69.7    | +2            |
| SagNet [49]     | $81.6 \pm 0.4^\uparrow$   | $62.7 \pm 0.4^\downarrow$ | $42.3 \pm 0.7$            | $95.0 \pm 0.2^\uparrow$   | 70.4    | +1            |
| <b>ERM</b> [68] | $81.5 \pm 0.0$            | $63.3 \pm 0.2$            | $42.6 \pm 0.9$            | $94.7 \pm 0.1$            | 70.5    | 0             |
| IGA [36]        | $80.9 \pm 0.4^\downarrow$ | $63.6 \pm 0.2^\uparrow$   | $41.3 \pm 0.8^\downarrow$ | $95.1 \pm 0.1^\uparrow$   | 70.2    | 0             |
| CORAL [64]      | $81.6 \pm 0.6^\uparrow$   | $63.8 \pm 0.3^\uparrow$   | $38.3 \pm 0.7^\downarrow$ | $94.2 \pm 0.3^\downarrow$ | 69.5    | 0             |
| IRM [7]         | $81.1 \pm 0.3^\downarrow$ | $63.0 \pm 0.2^\downarrow$ | $42.0 \pm 1.8$            | $95.0 \pm 0.4^\uparrow$   | 70.3    | -1            |
| VREx [37]       | $81.8 \pm 0.1^\uparrow$   | $63.5 \pm 0.1$            | $40.7 \pm 0.7^\downarrow$ | $94.1 \pm 0.3^\downarrow$ | 70.0    | -1            |
| GroupDRO [62]   | $80.4 \pm 0.3^\downarrow$ | $63.2 \pm 0.2$            | $36.8 \pm 1.1^\downarrow$ | $95.2 \pm 0.2^\uparrow$   | 68.9    | -1            |
| ERDG [79]       | $80.5 \pm 0.5^\downarrow$ | $63.0 \pm 0.4^\downarrow$ | $41.3 \pm 1.2^\downarrow$ | $95.5 \pm 0.2^\uparrow$   | 70.1    | -2            |
| DANN [24]       | $81.1 \pm 0.4^\downarrow$ | $62.9 \pm 0.6^\downarrow$ | $39.5 \pm 0.2^\downarrow$ | $94.9 \pm 0.0^\uparrow$   | 69.6    | -2            |
| MTL [15]        | $81.2 \pm 0.4^\downarrow$ | $62.9 \pm 0.2^\downarrow$ | $38.9 \pm 0.6^\downarrow$ | $95.0 \pm 0.1^\uparrow$   | 69.5    | -2            |
| Mixup [76]      | $79.8 \pm 0.6^\downarrow$ | $63.3 \pm 0.5$            | $39.8 \pm 0.3^\downarrow$ | $94.6 \pm 0.3$            | 69.4    | -2            |
| ANDMask [51]    | $79.5 \pm 0.0^\downarrow$ | $62.0 \pm 0.3^\downarrow$ | $39.8 \pm 1.4^\downarrow$ | $95.3 \pm 0.1^\uparrow$   | 69.2    | -2            |
| ARM [78]        | $81.0 \pm 0.4^\downarrow$ | $63.2 \pm 0.2$            | $39.4 \pm 0.7^\downarrow$ | $93.5 \pm 0.6^\downarrow$ | 69.3    | -3            |
| MLDG [40]       | $73.0 \pm 0.4^\downarrow$ | $52.4 \pm 0.2^\downarrow$ | $27.4 \pm 2.0^\downarrow$ | $91.2 \pm 0.4^\downarrow$ | 61.0    | -4            |
| <b>Average</b>  | 80.7                      | 62.5                      | 39.8                      | 94.6                      | 69.4    | -             |

Table 2: Performance of ERM and OoD generalization algorithms on datasets *dominated by correlation shift*. Every symbol  $\downarrow$  denotes a score of -1, and every symbol  $\uparrow$  denotes a score of +1; otherwise the score is 0. Adding up the scores across all datasets produces the ranking score for each algorithm.

| Algorithm       | Colored MNIST             | CelebA                    | NICO                      | Average | Prev score | Ranking score |
|-----------------|---------------------------|---------------------------|---------------------------|---------|------------|---------------|
| VREx [37]       | $56.3 \pm 1.9^\uparrow$   | $87.3 \pm 0.2$            | $71.0 \pm 1.3$            | 71.5    | -1         | +1            |
| GroupDRO [62]   | $32.5 \pm 0.2^\uparrow$   | $87.5 \pm 1.1$            | $71.8 \pm 0.8$            | 63.9    | -1         | +1            |
| <b>ERM</b> [68] | $29.9 \pm 0.9$            | $87.2 \pm 0.6$            | $71.4 \pm 1.3$            | 62.8    | 0          | 0             |
| MTL [15]        | $29.3 \pm 0.1$            | $87.0 \pm 0.7$            | $70.2 \pm 0.6$            | 62.2    | -2         | 0             |
| ERDG [79]       | $31.6 \pm 1.3^\uparrow$   | $84.5 \pm 0.2^\downarrow$ | $70.6 \pm 1.3$            | 62.2    | -2         | 0             |
| ARM [78]        | $34.6 \pm 1.8^\uparrow$   | $86.6 \pm 0.7$            | $63.9 \pm 1.8^\downarrow$ | 61.7    | -3         | 0             |
| MMD [41]        | $50.7 \pm 0.1^\uparrow$   | $86.0 \pm 0.5^\downarrow$ | $68.3 \pm 1.0^\downarrow$ | 68.3    | +2         | -1            |
| IGA [36]        | $29.7 \pm 0.5$            | $86.2 \pm 0.7^\downarrow$ | $70.5 \pm 1.2$            | 62.1    | 0          | -1            |
| IRM [7]         | $60.2 \pm 2.4^\uparrow$   | $85.4 \pm 1.2^\downarrow$ | $67.6 \pm 1.4^\downarrow$ | 71.1    | -1         | -1            |
| MLDG [40]       | $32.7 \pm 1.1^\uparrow$   | $85.4 \pm 1.3^\downarrow$ | $51.6 \pm 6.1^\downarrow$ | 56.6    | -4         | -1            |
| SagNet [49]     | $30.5 \pm 0.7$            | $85.8 \pm 1.4^\downarrow$ | $69.3 \pm 1.0^\downarrow$ | 61.9    | +1         | -2            |
| CORAL [64]      | $30.0 \pm 0.5$            | $86.3 \pm 0.5^\downarrow$ | $68.3 \pm 1.4^\downarrow$ | 61.5    | -1         | -2            |
| ANDMask [51]    | $27.2 \pm 1.4^\downarrow$ | $86.2 \pm 0.2^\downarrow$ | $72.2 \pm 1.2$            | 61.9    | -2         | -2            |
| Mixup [76]      | $27.6 \pm 1.8^\downarrow$ | $87.5 \pm 0.5$            | $66.6 \pm 0.9^\downarrow$ | 60.6    | -2         | -2            |
| RSC [34]        | $28.6 \pm 1.5^\downarrow$ | $85.9 \pm 0.2^\downarrow$ | $69.7 \pm 0.3^\downarrow$ | 61.4    | +2         | -3            |
| DANN [24]       | $24.5 \pm 0.8^\downarrow$ | $86.0 \pm 0.4^\downarrow$ | $68.6 \pm 1.1^\downarrow$ | 59.7    | -2         | -3            |
| <b>Average</b>  | 34.5                      | 68.4                      | 86.4                      | 63.1    | -          | -             |



**Results** The benchmark results are shown in Table 1 and Table 2. In addition to mean accuracy and standard error bar, we report a ranking score for each algorithm with respect to ERM. For every dataset-algorithm pair, depending on whether the attained accuracy is lower than, within, or higher than the standard error bar of ERM accuracy on the same dataset, we assign score -1, 0, +1 to the pair. Adding up the scores across all datasets listed in the table produces the ranking score for each algorithm. We underline that the ranking score does not indicate whether an algorithm is definitely better or worse than the other algorithms, but it only reflects a relative degree of robustness against diversity and correlation shift.

**Analysis** From Table 1 and Table 2, we observe that it is hard for most existing OoD generalization algorithms to achieve consistently better performance than ERM on both OoD directions. For example, on the datasets dominated by diversity shift in Table 1, the ranking scores of MMD, RSC, IGA, and SagNet are higher than ERM, whereas on the datasets dominated by correlation shift, their scores are lower. Conversely, the algorithms (GroupDRO and VREx) that outperform ERM in Table 2 are worse than ERM on datasets of the other kind. This supports our view that *OoD generalization algorithms should be evaluated on datasets embodying both diversity and correlation shift*. Such a comprehensive evaluation is of great importance because real-world data could be tainted by both kinds of distribution shift, e.g., the ImageNet variants listed in Figure 3.

Based on our previous estimation in Figure 3, among the four datasets dominated by diversity shift in Table 1, OfficeHome is the only one that also has a certain degree of correlation shift. This might explain why RSC and SagNet have -1 scores only on OfficeHome in Table 1 (as they both have low ranking scores in Table 2). In the toy case of Colored MNIST, several algorithms are superior to ERM, however, in the more realistic and complicated cases of CelebA and NICO, none of the algorithms surpasses ERM by a proper margin. Consequently, we argue that *contemporary OoD generalization algorithms are by large still vulnerable to spurious correlations*. In particular, IRM that achieves the best accuracy on Colored MNIST among all algorithms, fails to generalize well on the other two datasets. It is in line with the theoretical results discovered by Rosenfeld et al. [60]: IRM does not improve over ERM unless the test data are sufficiently similar to the training distribution.

Due to inevitable noises and other changing factors in the chosen datasets and training process, whether there is any compelling similarity or pattern in the results across the datasets dominated by the same kind of distribution shift is unclear. So, it is important to point out that the magnitude of diversity and correlation shift does not indicate the absolute level of difficulty for generalization. Instead, it represents a likelihood that certain algorithms will perform better than some other algorithms under the same kind of distribution shift.

### 3.2 Interpretation of learned representations

In this section, we provide interpretable visualizations of deep neural networks trained by different algorithms to gain a better understanding of the differences in learned representations. Due to space constraints, we have only selected two leading algorithms: RSC for diversity shift and VREx for correlation shift in comparison with ERM. In Figure 4, the left two columns are samples from the photo domain of PACS while the models are trained on the other three domains. RSC outperforms ERM and VREx in Table 1 as it has broader attention and therefore captures more global structural information rather than local details.

The two columns on the right are samples from NICO (dominated by correlation shift). In these cases, the attention of RSC has been diverted from the targets of interest by non-causal and local features like backgrounds and body parts. In contrast, ERM attends to more regions including the targets, while the attention of VREx is even more diverse, covering distinct regions scattered throughout the images. Moreover, the weak intensity of attention suggests that VREx is less prone to be overconfident on spurious correlations.

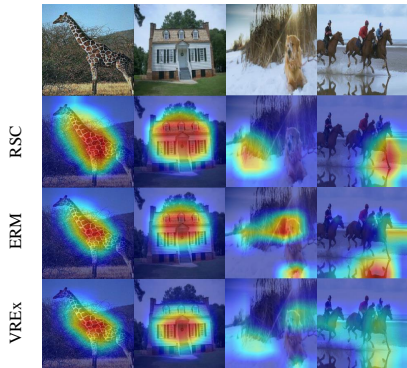


Figure 4: Attention heatmaps of selected algorithms trained and evaluated on PACS and NICO visualized by EigenCAM [48].

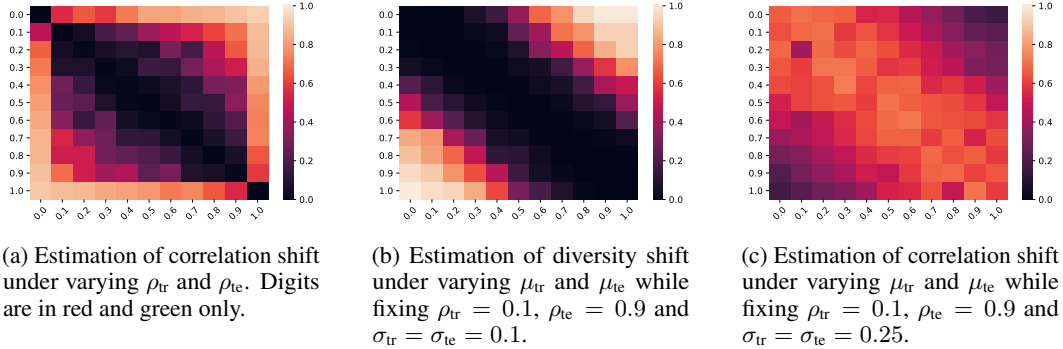


Figure 5: Estimation of diversity and correlation shift under varying color distribution in Colored MNIST. Another color, blue, uncorrelated with the labeled classes, is added onto the digits to create diversity shift. The intensity of blue is sampled from a truncated Gaussian distribution for every image. Assuming only one training and one test environment,  $\rho_{tr}$  and  $\rho_{te}$  stand for the correlation between red/green and the digits;  $\mu_{tr}$  and  $\mu_{te}$  stand for the mean intensities of blue;  $\sigma_{tr}$  and  $\sigma_{te}$  stand for the standard deviations.

### 3.3 Ablation study

In this section, we conduct ablation study to check the reliability of our estimation method for diversity and correlation shift and compare it against other existing metrics for measuring the non-i.i.d. property of datasets.

**Estimation of diversity and correlation shift** To validate the robustness of our estimation method, we conduct ablation study on Colored MNIST to check whether it can produce results that faithfully reflect expected trends as we manipulate the color distribution. For simplicity, only one training environment is used. For correlation shift, we manipulate the correlation coefficients  $\rho_{tr}$  and  $\rho_{te}$  between digits and colors in constructing the dataset. From Figure 5a, we can observe that when  $\rho_{tr}$  and  $\rho_{te}$  have similar values, the estimated correlation shift is negligible. It aligns well with our definition of correlation shift that measures the distribution difference of features present in both environments.

As for checking on the estimation of diversity shift, another color, blue, is introduced in the dataset. The intensity (between 0 and 1) of blue added onto each digit is sampled from truncated Gaussian distributions with means  $\mu_{tr}$ ,  $\mu_{te}$  and standard deviations  $\sigma_{tr}$ ,  $\sigma_{te}$  for training and test environment respectively. Meanwhile, the intensity of red and green is subtracted by the same amount. From Figure 5b, we can observe that as the color difference varies between red/green and blue, the estimate of diversity shift varies accordingly (at the corners).

Lastly, we investigate the behavior in the estimation of correlation shift while keeping the correlation coefficients fixed and manipulating  $\mu_{tr}$  and  $\mu_{te}$  that controls diversity shift. Figure 5c shows a trade-off between diversity and correlation shift, as implied by their definitions. Experiments in every grid cell are conducted only once, so the heatmaps also reflect the variance in our estimation, which can be compensated by averaging over multiple runs.

**Comparison with other measures of distribution shift** We also compare OoD-Bench with other measures of distribution shift. The results on the variants of Colored MNIST are shown in Table 3. We empirically show that general metrics for measuring the discrepancy between distributions, such as EMD [61] and MMD [26], can fail to provide informative knowledge on the distribution shifts in OoD datasets. Specifically, EMD and MMD are insensitive to the correlation shift in the datasets, while EMD is also insensitive to the diversity shift. Although NI [29] can produce comparative results on correlation shift, it is still unidimensional like EMD and MMD, which cannot discern the two kinds of distribution shift present in the datasets. Our method provides more stable and interpretable results in comparison. As  $\rho_{tr}$  and  $\rho_{te}$  gradually become close, the estimated correlation shift reduces to zero. On the other hand, the estimated diversity shift remains constant zero until the last scenario where our method again produces the expected answer.



Table 3: Existing metrics on measuring the distribution shift in Colored MNIST with only one training environment where  $\rho_{tr} = 0.1$ . All environments contain only red and green digits except the last. <sup>†</sup>Blue is added with  $\mu_{tr} = 0$ ,  $\mu_{te} = 1$  and  $\sigma_{tr} = \sigma_{te} = 0.1$ . Results are averaged over 5 runs.

| $\rho_{te}$      | Dominant shift | EMD               | MMD               | NI                 | Div. shift (ours) | Cor. shift (ours) |
|------------------|----------------|-------------------|-------------------|--------------------|-------------------|-------------------|
| 0.9              | Cor. shift     | $0.08 \pm 0.01$ ✗ | $0.01 \pm 0.00$ ✗ | $1.40 \pm 0.06$ ✓  | $0.00 \pm 0.00$   | $0.67 \pm 0.04$   |
| 0.7              | Cor. shift     | $0.07 \pm 0.00$ ✗ | $0.01 \pm 0.00$ ✗ | $1.05 \pm 0.03$ ✓  | $0.00 \pm 0.00$   | $0.48 \pm 0.06$   |
| 0.5              | Cor. shift     | $0.07 \pm 0.00$ ✗ | $0.00 \pm 0.00$ ✗ | $0.72 \pm 0.04$ ✓  | $0.00 \pm 0.00$   | $0.34 \pm 0.06$   |
| 0.3              | Cor. shift     | $0.06 \pm 0.00$ ✗ | $0.00 \pm 0.00$ ✗ | $0.57 \pm 0.04$ ✓  | $0.00 \pm 0.00$   | $0.18 \pm 0.05$   |
| 0.1              | None           | $0.06 \pm 0.00$ ✗ | $0.00 \pm 0.00$ ✓ | $0.39 \pm 0.02$ ✗  | $0.00 \pm 0.00$   | $0.00 \pm 0.00$   |
| 0.1 <sup>†</sup> | Div. shift     | $0.29 \pm 0.01$ ✗ | $1.00 \pm 0.00$ ✓ | $10.76 \pm 0.43$ ✗ | $0.93 \pm 0.01$   | $0.00 \pm 0.00$   |

## 4 Related work

**Quantification on distribution shifts** He et al. [29] propose the Non-I.I.D. Index (NI) to quantify the degree of distribution shift between training and testing sets. The metric is based on the difference between the outputs of the penultimate layer on the training set and those of the testing set. This one-dimensional shift measurement cannot explain why many OoD generalization algorithms fail on the Colored MNIST. There are also a great number of general distance measures for distributions: Kullback-Leibler (KL) divergence, EMD [61], MMD [26], and  $\mathcal{A}$ -distance [13], etc. However, they also suffer from the same problem as NI, not being able to discern different kinds of distribution shifts. To the best of our knowledge, we are the first to formally define the two-dimensional distribution shift and provide quantitative results on various OoD datasets.

**OoD generalization algorithms** Currently, there are two main streams of research on OoD generalization algorithms in deep learning: Domain Generalization (DG) and risk regularization methods. DG has been an active research area for quite some time, dating back to the work of Torralba and Efros [67]. It has since then sprouted into a number of branches such as invariant representation learning [47, 41, 42, 3, 5], meta-learning for DG [40, 11, 23, 43], and data augmentation for DG [71, 77, 73, 72, 80]. The seminal work of risk regularization methods, IRM [7], aims to find an invariant representation of data from different training environments by adding an invariant risk regularization. It has thereafter inspired several other notable algorithms, including IRM-Games [1], VREx [37] and IGA [36].

**DomainBed** The living benchmark is created by Gulrajani and Lopez-Paz [27] to facilitate disciplined and reproducible DG research. After conducting a large-scale hyperparameter search, the performances of fourteen algorithms on seven datasets are reported in the paper. The authors then arrive at the conclusion that ERM beats most of DG algorithms under the same fair setting. Our work differs from DomainBed mainly in three aspects. First, we not only provide a benchmark for algorithms but also for datasets, helping us gain a deeper understanding of the distribution shift in the data that are used to train and evaluate the algorithms. Second, we compare different algorithms in a more informative manner in light of diversity and correlation shift, recovering the fact that some algorithms are indeed better than ERM in appropriate scenarios. Third, we experiment with several new algorithms and new datasets, especially those dominated by correlation shift.

## 5 Conclusion

In this paper, we have identified diversity shift and correlation shift as two of the main forms of distribution shift in OoD datasets. The two-dimensional characterization positions disconnected datasets into a unified picture and have shed light on the nature of unknown distribution shift in some real-world data. In addition, we have demonstrated some of the strengths and weaknesses of existing OoD generalization algorithms. The results suggest that future algorithms should be more comprehensively evaluated on two types of datasets, one dominated by diversity shift and the other dominated by correlation shift. Last but not least, we have left an open problem regarding whether there exists an algorithm that can perform simultaneously well under diversity and correlation shift. If not then our method can be used for choosing the appropriate algorithms.

## References

- [1] Kartik Ahuja, Karthikeyan Shanmugam, Kush Varshney, and Amit Dhurandhar. Invariant risk minimization games. In *ICML*, 2020.
- [2] Kartik Ahuja, Jun Wang, Amit Dhurandhar, Karthikeyan Shanmugam, and Kush R. Varshney. Empirical or invariant risk minimization? a sample complexity perspective. In *ICLR*, 2021.
- [3] Kei Akuzawa, Yusuke Iwasawa, and Yutaka Matsuo. Adversarial invariant feature learning with accuracy constraint for domain generalization. In *ECML-PKDD*, 2019.
- [4] Ehab A AlBadawy, Ashirbani Saha, and Maciej A Mazurowski. Deep learning for segmentation of brain tumors: Impact of cross-institutional training and testing. *Medical physics*, 2018.
- [5] Isabela Albuquerque, João Monteiro, Tiago H Falk, and Ioannis Mitliagkas. Adversarial target-invariant representation learning for domain generalization. *arXiv:1911.00804*, 2019.
- [6] Michael A Alcorn, Qi Li, Zhitao Gong, Chengfei Wang, Long Mai, Wei-Shinn Ku, and Anh Nguyen. Strike (with) a pose: Neural networks are easily fooled by strange poses of familiar objects. In *CVPR*, 2019.
- [7] Martin Arjovsky, Léon Bottou, Ishaan Gulrajani, and David Lopez-Paz. Invariant risk minimization. *arXiv:1907.02893*, 2019.
- [8] Kamyar Azizzadenesheli, Anqi Liu, Fanny Yang, and Animashree Anandkumar. Regularized learning for domain adaptation under label shifts. In *ICLR*, 2019.
- [9] Hyojin Bahng, Sanghyuk Chun, Sangdoon Yun, Jaegul Choo, and Seong Joon Oh. Learning de-biased representations with biased representations. In *ICML*, 2020.
- [10] Haoyue Bai, Rui Sun, Lanqing Hong, Fengwei Zhou, Nanyang Ye, Han-Jia Ye, S-H Gary Chan, and Zhenguo Li. Decaug: Out-of-distribution generalization via decomposed feature representation and semantic augmentation. *arXiv:2012.09382*, 2020.
- [11] Yogesh Balaji, Swami Sankaranarayanan, and Rama Chellappa. Metareg: Towards domain generalization using meta-regularization. *NeurIPS*, 2018.
- [12] Sara Beery, Grant Van Horn, and Pietro Perona. Recognition in terra incognita. In *ECCV*, 2018.
- [13] Shai Ben-David, John Blitzer, Koby Crammer, Fernando Pereira, et al. Analysis of representations for domain adaptation. *NeurIPS*, 2007.
- [14] Gilles Blanchard, Gyemin Lee, and Clayton Scott. Generalizing from several related classification tasks to a new unlabeled sample. In *NeurIPS*, 2011.
- [15] Gilles Blanchard, Aniket Anand Deshmukh, Urun Dogan, Gyemin Lee, and Clayton Scott. Domain generalization by marginal transfer learning. *arXiv:1711.07910*, 2017.
- [16] Péter et al. Bándi. From detection of individual metastases to classification of lymph node status at the patient level: The CAMELYON17 challenge. *TMI*, 2019.
- [17] Fabio Maria Carlucci, Antonio D’Innocente, Silvia Bucci, Barbara Caputo, and Tatiana Tommasi. Domain generalization by solving jigsaw puzzles. In *CVPR*, 2019.
- [18] Daniel C Castro, Ian Walker, and Ben Glocker. Causality matters in medical imaging. *Nature Communications*, 2020.
- [19] Ching-Yao Chuang and Youssef Mroueh. Fair mixup: Fairness via interpolation. In *ICLR*, 2021.
- [20] Dengxin Dai and Luc Van Gool. Dark model adaptation: Semantic image segmentation from daytime to nighttime. In *ITSC*, 2018.
- [21] Jia Deng, Wei Dong, Richard Socher, Li-Jia Li, Kai Li, and Li Fei-Fei. Imagenet: A large-scale hierarchical image database. In *CVPR*, 2009.
- [22] Jacob Devlin, Ming-Wei Chang, Kenton Lee, and Kristina Toutanova. Bert: Pre-training of deep bidirectional transformers for language understanding. *arXiv:1810.04805*, 2018.
- [23] Qi Dou, Daniel C. Castro, Konstantinos Kamnitsas, and Ben Glocker. Domain generalization via model-agnostic learning of semantic features. In *NeurIPS*, 2019.

- [24] Yaroslav Ganin, Evgeniya Ustinova, Hana Ajakan, Pascal Germain, Hugo Larochelle, François Laviolette, Mario Marchand, and Victor Lempitsky. Domain-adversarial training of neural networks. *JMLR*, 2016.
- [25] Robert Geirhos, Jörn-Henrik Jacobsen, Claudio Michaelis, Richard Zemel, Wieland Brendel, Matthias Bethge, and Felix A. Wichmann. Shortcut learning in deep neural networks. *Nature Machine Intelligence*, 2020.
- [26] Arthur Gretton, Karsten Borgwardt, Malte Rasch, Bernhard Schölkopf, and Alex Smola. A kernel method for the two-sample-problem. *NeurIPS*, 2006.
- [27] Ishaan Gulrajani and David Lopez-Paz. In search of lost domain generalization. In *ICLR*, 2021.
- [28] Kaiming He, Xiangyu Zhang, Shaoqing Ren, and Jian Sun. Deep residual learning for image recognition. In *CVPR*, 2016.
- [29] Yue He, Zheyang Shen, and Peng Cui. Towards non-iid image classification: A dataset and baselines. *Pattern Recognition*, 2020.
- [30] Ernst Hellinger. Neue begründung der theorie quadratischer formen von unendlichvielen veränderlichen. *Journal für die reine und angewandte Mathematik*, 1909.
- [31] Dan Hendrycks, Kevin Zhao, Steven Basart, Jacob Steinhardt, and Dawn Song. Natural adversarial examples. *arXiv:1907.07174*, 2019.
- [32] Dan Hendrycks, Steven Basart, Norman Mu, Saurav Kadavath, Frank Wang, Evan Dorundo, Rahul Desai, Tyler Zhu, Samyak Parajuli, Mike Guo, Dawn Song, Jacob Steinhardt, and Justin Gilmer. The many faces of robustness: A critical analysis of out-of-distribution generalization. *arXiv:2006.16241*, 2020.
- [33] Xiaowei Huang, Daniel Kroening, Wenjie Ruan, James Sharp, Youcheng Sun, Emese Thamo, Min Wu, and Xinpeng Yi. A survey of safety and trustworthiness of deep neural networks: Verification, testing, adversarial attack and defence, and interpretability. *Computer Science Review*, 2020.
- [34] Zeyi Huang, Haohan Wang, Eric P Xing, and Dong Huang. Self-challenging improves cross-domain generalization. *arXiv:2007.02454*, 2020.
- [35] Pang Wei Koh, Shiori Sagawa, Henrik Marklund, Sang Michael Xie, Marvin Zhang, Akshay Balsubramani, Weihua Hu, Michihiro Yasunaga, Richard Lanus Phillips, Sara Beery, et al. Wilds: A benchmark of in-the-wild distribution shifts. *arXiv:2012.07421*, 2020.
- [36] Masanori Koyama and Shoichiro Yamaguchi. Out-of-distribution generalization with maximal invariant predictor. *arXiv:2008.01883*, 2020.
- [37] David Krueger, Ethan Caballero, Joern-Henrik Jacobsen, Amy Zhang, Jonathan Binas, Remi Le Priol, and Aaron Courville. Out-of-distribution generalization via risk extrapolation (rex). *arXiv:2003.00688*, 2020.
- [38] Y. Lecun, L. Bottou, Y. Bengio, and P. Haffner. Gradient-based learning applied to document recognition. *Proceedings of the IEEE*, 1998.
- [39] D. Li, Y. Yang, Y. Song, and T. M. Hospedales. Deeper, broader and artier domain generalization. In *ICCV*, 2017.
- [40] Da Li, Yongxin Yang, Yi-Zhe Song, and Timothy Hospedales. Learning to generalize: Meta-learning for domain generalization. In *AAAI*, 2018.
- [41] Haoliang Li, Sinno Jialin Pan, Shiqi Wang, and Alex C Kot. Domain generalization with adversarial feature learning. In *CVPR*, 2018.
- [42] Ya Li, Mingming Gong, Xinmei Tian, Tongliang Liu, and Dacheng Tao. Domain generalization via conditional invariant representations. In *AAAI*, 2018.
- [43] Yiyang Li, Yongxin Yang, Wei Zhou, and Timothy Hospedales. Feature-critic networks for heterogeneous domain generalization. In *ICML*, 2019.
- [44] Chang Liu, Xinwei Sun, Jindong Wang, Haoyue Tang, Tao Li, Tao Qin, Wei Chen, and Tie-Yan Liu. Learning causal semantic representation for out-of-distribution prediction. *arXiv:2011.01681*, 2020.
- [45] Ziwei Liu, Ping Luo, Xiaogang Wang, and Xiaoou Tang. Deep learning face attributes in the wild. In *ICCV*, 2015.

- [46] Massimiliano Mancini, Zeynep Akata, Elisa Ricci, and Barbara Caputo. Towards recognizing unseen categories in unseen domains. In *ECCV*, 2020.
- [47] Krikamol Muandet, David Balduzzi, and Bernhard Schölkopf. Domain generalization via invariant feature representation. In *ICML*, 2013.
- [48] Mohammed Bany Muhammad and Mohammed Yeasin. Eigen-cam: Class activation map using principal components. In *IJCNN*, 2020.
- [49] Hyeonseob Nam, HyunJae Lee, Jongchan Park, Wonjun Yoon, and Donggeun Yoo. Reducing domain gap via style-agnostic networks. *arXiv:1910.11645*, 2019.
- [50] M Newman and G Barkema. *Monte carlo methods in statistical physics chapter 1-4*. Oxford University Press, 1999.
- [51] Giambattista Parascandolo, Alexander Neitz, ANTONIO ORVIETO, Luigi Gresele, and Bernhard Schölkopf. Learning explanations that are hard to vary. In *ICLR*, 2021.
- [52] Emanuel Parzen. On estimation of a probability density function and mode. *The Annals of Mathematical Statistics*, 1962.
- [53] Judea Pearl. *Causality: Models, Reasoning and Inference*. Cambridge University Press, 2000.
- [54] Xingchao Peng, Qinxun Bai, Xide Xia, Zijun Huang, Kate Saenko, and Bo Wang. Moment matching for multi-source domain adaptation. In *ICCV*, 2019.
- [55] Mohammad Pezeshki, Sékou-Oumar Kaba, Yoshua Bengio, Aaron Courville, Doina Precup, and Guillaume Lajoie. Gradient starvation: A learning proclivity in neural networks. *arXiv:2011.09468*, 2020.
- [56] Novi Quadrianto, Viktoriia Sharmanska, and Oliver Thomas. Discovering fair representations in the data domain. In *CVPR*, 2019.
- [57] Benjamin Recht, Rebecca Roelofs, Ludwig Schmidt, and Vaishaal Shankar. Do ImageNet classifiers generalize to ImageNet? In *ICML*, 2019.
- [58] Benjamin Recht, Rebecca Roelofs, Ludwig Schmidt, and Vaishaal Shankar. Do imagenet classifiers generalize to imagenet? In *ICML*, 2019.
- [59] Murray Rosenblatt. Remarks on some nonparametric estimates of a density function. *The Annals of Mathematical Statistics*, 1956.
- [60] Elan Rosenfeld, Pradeep Kumar Ravikumar, and Andrej Risteski. The risks of invariant risk minimization. In *ICLR*, 2021.
- [61] Yossi Rubner, Carlo Tomasi, and Leonidas J Guibas. A metric for distributions with applications to image databases. In *ICCV*, 1998.
- [62] Shiori Sagawa, Pang Wei Koh, Tatsunori B. Hashimoto, and Percy Liang. Distributionally robust neural networks. In *ICLR*, 2020.
- [63] Takami Sato, Junjie Shen, Ningfei Wang, Yunhan Jack Jia, Xue Lin, and Qi Alfred Chen. Security of deep learning based lane keeping system under physical-world adversarial attack. *arXiv:2003.01782*, 2020.
- [64] Baochen Sun and Kate Saenko. Deep coral: Correlation alignment for deep domain adaptation. In *ECCV*, 2016.
- [65] Yu Sun, Xiaolong Wang, Zhuang Liu, John Miller, Alexei Efros, and Moritz Hardt. Test-time training with self-supervision for generalization under distribution shifts. In *ICML*, 2020.
- [66] Christian Szegedy, Wojciech Zaremba, Ilya Sutskever, Joan Bruna, Dumitru Erhan, Ian Goodfellow, and Rob Fergus. Intriguing properties of neural networks. In *ICLR*, 2014.
- [67] Antonio Torralba and Alexei A. Efros. Unbiased look at dataset bias. In *CVPR*, 2011.
- [68] Vladimir Vapnik. *Statistical Learning Theory*. Wiley, 1998.
- [69] Hemanth Venkateswara, Jose Eusebio, Shayok Chakraborty, and Sethuraman Panchanathan. Deep hashing network for unsupervised domain adaptation. In *CVPR*, 2017.
- [70] Georg Volk, Stefan Müller, Alexander von Bernuth, Dennis Hospach, and Oliver Bringmann. Towards robust CNN-based object detection through augmentation with synthetic rain variations. In *ITSC*, 2019.

- [71] Riccardo Volpi, Hongseok Namkoong, Ozan Sener, John Duchi, Vittorio Murino, and Silvio Savarese. Generalizing to unseen domains via adversarial data augmentation. *arXiv:1805.12018*, 2018.
- [72] Shujun Wang, Lequan Yu, Caizi Li, Chi-Wing Fu, and Pheng-Ann Heng. Learning from extrinsic and intrinsic supervisions for domain generalization. In *ECCV*, 2020.
- [73] Yufei Wang, Haoliang Li, and Alex C Kot. Heterogeneous domain generalization via domain mixup. In *ICASSP*, 2020.
- [74] Zeyu Wang, Klint Qinami, Ioannis Karakozis, Kyle Genova, Prem Nair, Kenji Hata, and Olga Russakovsky. Towards fairness in visual recognition: Effective strategies for bias mitigation. In *CVPR*, 2020.
- [75] Minghao Xu, Jian Zhang, Bingbing Ni, Teng Li, Chengjie Wang, Qi Tian, and Wenjun Zhang. Adversarial domain adaptation with domain mixup. In *AAAI*, 2020.
- [76] Shen Yan, Huan Song, Nanxiang Li, Lincan Zou, and Liu Ren. Improve unsupervised domain adaptation with mixup training, 2020.
- [77] Ling Zhang, Xiaosong Wang, Dong Yang, Thomas Sanford, Stephanie Harmon, Baris Turkbey, Holger Roth, Andriy Myronenko, Daguang Xu, and Ziyue Xu. When unseen domain generalization is unnecessary? rethinking data augmentation. *arXiv:1906.03347*, 2019.
- [78] Marvin Zhang, Henrik Marklund, Nikita Dhawan, Abhishek Gupta, Sergey Levine, and Chelsea Finn. Adaptive risk minimization: A meta-learning approach for tackling group distribution shift. *arXiv:2007.02931*, 2020.
- [79] Shanshan Zhao, Mingming Gong, Tongliang Liu, Huan Fu, and Dacheng Tao. Domain generalization via entropy regularization. *NeurIPS*, 2020.
- [80] Kaiyang Zhou, Yongxin Yang, Timothy Hospedales, and Tao Xiang. Deep domain-adversarial image generation for domain generalisation. In *AAAI*, 2020.
- [81] Kaiyang Zhou, Ziwei Liu, Yu Qiao, Tao Xiang, and Chen Change Loy. Domain generalization: A survey. *arXiv:2103.02503*, 2021.

## A Proofs

In this work, we only make one mild assumption that holds in most existing datasets and can be easily enforced when it does not. In Algorithm 1, we adopt a weighted sampling strategy in order to always meet the assumption, though there are many other possible approaches which do not affect our conclusion. The assumption will be used in the proofs of the propositions followed.

**Assumption 1.** For every  $\mathbf{y} \in \mathcal{Y}$ ,  $p(\mathbf{y}) = q(\mathbf{y}) > 0$ , i.e., there is no label shift.

The first proposition proves the bound on diversity and correlation shift mentioned in Section 2.

**Proposition 1.** For any non-negative probability functions  $p$  and  $q$ , diversity shift  $d_{\text{div}}(p, q)$  and correlation shift  $d_{\text{cor}}(p, q)$  are always bounded between 0 and 1, inclusively.

*Proof.* Apparently,  $d_{\text{div}}(p, q)$  and  $d_{\text{cor}}(p, q)$  are always non-negative, so then we only need to prove the upper bound. By the triangle inequality and that every probability function sums up to one over all possible outcomes,

$$d_{\text{div}}(p, q) = \frac{1}{2} \int_{\mathcal{S}} |p(\mathbf{z}_2) - q(\mathbf{z}_2)| d^m \mathbf{z}_2 \leq \frac{1}{2} \int_{\mathcal{S}} [p(\mathbf{z}_2) + q(\mathbf{z}_2)] d^m \mathbf{z}_2 \leq 1. \quad (6)$$

Similarly, we have

$$\begin{aligned} d_{\text{cor}}(p, q) &= \frac{1}{2} \int_{\mathcal{T}} \sqrt{p(\mathbf{z}_2) q(\mathbf{z}_2)} \sum_{\mathbf{y} \in \mathcal{Y}} |p(\mathbf{y} | \mathbf{z}_2) - q(\mathbf{y} | \mathbf{z}_2)| d^m \mathbf{z}_2 \\ &\leq \frac{1}{2} \int_{\mathcal{T}} \sqrt{p(\mathbf{z}_2) q(\mathbf{z}_2)} \sum_{\mathbf{y} \in \mathcal{Y}} [p(\mathbf{y} | \mathbf{z}_2) + q(\mathbf{y} | \mathbf{z}_2)] d^m \mathbf{z}_2 \\ &= \frac{1}{2} \int_{\mathcal{T}} 2\sqrt{p(\mathbf{z}_2) q(\mathbf{z}_2)} d^m \mathbf{z}_2 \leq \frac{1}{2} \int_{\mathcal{T}} [p(\mathbf{z}_2) + q(\mathbf{z}_2)] d^m \mathbf{z}_2 \leq 1. \end{aligned} \quad (7)$$

□

The following propositions will play a role in Appendix B.1, where we justify the design of our method for estimating diversity and correlation shift. Relevant notations are also introduced in Appendix B.1.

**Proposition 2.**  $\mathcal{Z}'_2 \subseteq \mathcal{U}$ , i.e., the practical representation of  $\mathcal{Z}_2$  is contained in the extracted features.

*Proof.* The proposition is equivalent to that  $\mathbf{z} \in \mathcal{Z}'_2 \implies \mathbf{z} \in \mathcal{U}$ . For simplicity, we prove the contrapositive statement:  $\mathbf{z} \notin \mathcal{Z}'_2 \iff \mathbf{z} \notin \mathcal{U}$ . Given  $\mathbf{z} \notin \mathcal{U}$ , by definition it is clear that  $\forall \mathbf{y} \in \mathcal{Y} : p(\mathbf{z} | \mathbf{y}) = q(\mathbf{z} | \mathbf{y})$  and at least one of  $p(\mathbf{z})$  or  $q(\mathbf{z})$  is nonzero. Hence, we have

$$p(\mathbf{z}) = \sum_{\mathbf{y} \in \mathcal{Y}} p(\mathbf{y}, \mathbf{z}) = \sum_{\mathbf{y} \in \mathcal{Y}} p(\mathbf{z} | \mathbf{y}) p(\mathbf{y}) = \sum_{\mathbf{y} \in \mathcal{Y}} q(\mathbf{z} | \mathbf{y}) q(\mathbf{y}) = \sum_{\mathbf{y} \in \mathcal{Y}} q(\mathbf{y}, \mathbf{z}) = q(\mathbf{z}), \quad (8)$$

which then suggests that  $p(\mathbf{z}) \cdot q(\mathbf{z}) > 0$  and for all  $\mathbf{y} \in \mathcal{Y}$ ,

$$p(\mathbf{y} | \mathbf{z}) = \frac{p(\mathbf{y}, \mathbf{z})}{p(\mathbf{z})} = \frac{p(\mathbf{z} | \mathbf{y}) p(\mathbf{y})}{p(\mathbf{z})} = \frac{q(\mathbf{z} | \mathbf{y}) q(\mathbf{y})}{q(\mathbf{z})} = \frac{q(\mathbf{y}, \mathbf{z})}{q(\mathbf{z})} = q(\mathbf{y} | \mathbf{z}). \quad (9)$$

□

**Proposition 3.** The two integrals over  $\mathcal{S}'$  and  $\mathcal{S}^*$  are equal:

$$\int_{\mathcal{S}'} |p(\mathbf{z}) - q(\mathbf{z})| d^m \mathbf{z} = \int_{\mathcal{S}^*} |p(\mathbf{z}) - q(\mathbf{z})| d^m \mathbf{z}.$$

*Proof.* By definition, we can rewrite

$$\mathcal{S}' = \{\mathbf{z} \in \mathbb{R}^m \mid p(\mathbf{z}) \cdot q(\mathbf{z}) = 0\}. \quad (10)$$

Since  $\mathcal{S}' \subseteq \mathcal{Z}'_2 \subseteq \mathcal{U}$  (see Proposition 2) and  $\mathcal{U} \subseteq \mathbb{R}^m$ , we then have

$$\mathcal{S}' = \{\mathbf{z} \in \mathcal{U} \mid p(\mathbf{z}) \cdot q(\mathbf{z}) = 0\} = \mathcal{S}^*. \quad (11)$$

□



**Proposition 4.** *The two integrals over  $\mathcal{T}'$  and  $\mathcal{T}^*$  are equal:*

$$\int_{\mathcal{T}'} \sqrt{p(\mathbf{z})q(\mathbf{z})} \sum_{\mathbf{y} \in \mathcal{Y}} |p(\mathbf{y} | \mathbf{z}) - q(\mathbf{y} | \mathbf{z})| d^m \mathbf{z} = \int_{\mathcal{T}^*} \sqrt{p(\mathbf{z})q(\mathbf{z})} \sum_{\mathbf{y} \in \mathcal{Y}} |p(\mathbf{y} | \mathbf{z}) - q(\mathbf{y} | \mathbf{z})| d^m \mathbf{z}.$$

*Proof.* Similar to the proof of Proposition 3, by reducing the definitions onto  $\mathbb{R}^m$ , we have

$$\mathcal{T}' = \{\mathbf{z} \in \mathbb{R}^m \mid p(\mathbf{z}) \cdot q(\mathbf{z}) \neq 0 \wedge \exists \mathbf{y} \in \mathcal{Y} : p(\mathbf{y} | \mathbf{z}) \neq q(\mathbf{y} | \mathbf{z})\}, \quad (12)$$

$$\mathcal{T}^* = \{\mathbf{z} \in \mathbb{R}^m \mid p(\mathbf{z}) \cdot q(\mathbf{z}) \neq 0 \wedge \exists \mathbf{y} \in \mathcal{Y} : p(\mathbf{z} | \mathbf{y}) \neq q(\mathbf{z} | \mathbf{y})\}, \quad (13)$$

and therefore the set difference

$$\begin{aligned} \mathcal{T}^* \setminus \mathcal{T}' = \{\mathbf{z} \in \mathbb{R}^m \mid p(\mathbf{z}) \cdot q(\mathbf{z}) \neq 0 \wedge \exists \mathbf{y} \in \mathcal{Y} : p(\mathbf{z} | \mathbf{y}) \neq q(\mathbf{z} | \mathbf{y}) \\ \wedge \forall \mathbf{y} \in \mathcal{Y} : p(\mathbf{y} | \mathbf{z}) = q(\mathbf{y} | \mathbf{z})\}. \end{aligned} \quad (14)$$

The last condition directly implies that  $\sum_{\mathbf{y} \in \mathcal{Y}} |p(\mathbf{y} | \mathbf{z}) - q(\mathbf{y} | \mathbf{z})| = 0$  for all  $\mathbf{z} \in \mathcal{T}^* \setminus \mathcal{T}'$ , and since it is easy to check that  $\mathcal{T}' \subseteq \mathcal{T}^*$ , the proposition is proved.  $\square$

## B Practical Estimation of Diversity and Correlation Shift

In this section, we provide complete pseudo codes of our OoD shifts estimation methods, supported by theoretical justifications. Executable Python codes are also included in the supplementary material.

### B.1 Pseudo codes and theoretical justifications

---

#### Algorithm 1 Training procedure of feature extractor

---

**Require:** Training environments  $\mathcal{E}_{\text{tr}} = \{\mathcal{E}_{\text{tr}}^1, \dots, \mathcal{E}_{\text{tr}}^a\}$  and test environments  $\mathcal{E}_{\text{te}} = \{\mathcal{E}_{\text{te}}^1, \dots, \mathcal{E}_{\text{te}}^b\}$ ; mini-batch size  $N$  per environment; number of training steps  $T$ ; feature dimension  $m$ .

**Ensure:** Feature extractor  $g_\phi : \mathcal{X} \rightarrow \mathbb{R}^m$ ; label mapping  $g'_\psi : \mathcal{Y} \rightarrow \mathbb{R}^m$ ; classifier  $h_\theta : \mathbb{R}^m \times \mathbb{R}^m \rightarrow \mathbb{R}^{a+b}$ .

- 1: Initialize network parameters  $\phi, \psi, \theta$ ;
  - 2: **for** each training step  $t \leftarrow 1, \dots, T$  **do**
  - 3:     **for** each environment  $\mathcal{E} \in \mathcal{E}_{\text{tr}} \cup \mathcal{E}_{\text{te}}$  **do**
  - 4:          $e \leftarrow$  the index of environment  $\mathcal{E}$ ;
  - 5:         sample a mini-batch of training examples  $\mathcal{D} = \{(\mathbf{x}_i, \mathbf{y}_i)\}_{i=1}^N$  from  $\mathcal{E}$  while ensuring equal sampling probability for every distinct value  $\mathbf{y} \in \mathcal{Y}$ ;  $\triangleright$  which then ensures Assumption 1
  - 6:         **for** each example  $(\mathbf{x}_i, \mathbf{y}_i) \in \mathcal{D}$  **do**
  - 7:              $\hat{\mathbf{e}} \leftarrow h_\theta(g_\phi(\mathbf{x}_i), g'_\psi(\mathbf{y}_i))$ ;
  - 8:             compute loss  $\ell(\hat{\mathbf{e}}, e)$  and accumulate gradient;  $\triangleright$  where  $\ell$  stands for the cross-entropy loss
  - 9:     update  $\phi, \psi, \theta$  by the accumulated gradient, and then reset the gradient.
- 

The training procedure of our feature extractor  $g_\phi$  (parameterized by  $\phi$ ) is described in Algorithm 1, where the output of  $g_\phi$  is assumed to be  $m$ -dimensional (or in  $\mathbb{R}^m$ ). Note that in line 5 of the pseudo code, we adopt a weighted sampling strategy to ensure the class balance in every environment so that Assumption 1 holds. As it is difficult to directly learn a representation of  $\mathcal{Z}_2$ , the whole purpose of Algorithm 1 is training  $g_\phi$  to learn a feature representation as follows:

$$\mathcal{U} = \{\mathbf{z} \in \mathbb{R}^m \mid p(\mathbf{z}) = q(\mathbf{z}) = 0 \vee \exists \mathbf{y} \in \mathcal{Y} : p(\mathbf{z} | \mathbf{y}) \neq q(\mathbf{z} | \mathbf{y})\}, \quad (15)$$

where  $p$  and  $q$  are the respective probability functions for the training and test environment. To see the reason, we need to introduce our estimators for diversity and correlation shift.

Similar to (1) and (2), we can also partition the outputs of  $g_\phi : \mathcal{X} \rightarrow \mathbb{R}^m$  into two sets:

$$\mathcal{Z}'_1 = \{\mathbf{z} \in \mathbb{R}^m \mid p(\mathbf{z}) \cdot q(\mathbf{z}) \neq 0 \wedge \forall \mathbf{y} \in \mathcal{Y} : p(\mathbf{y} | \mathbf{z}) = q(\mathbf{y} | \mathbf{z})\} \quad (16)$$

and

$$\mathcal{Z}'_2 = \{\mathbf{z} \in \mathbb{R}^m \mid p(\mathbf{z}) \cdot q(\mathbf{z}) = 0 \vee \exists \mathbf{y} \in \mathcal{Y} : p(\mathbf{y} | \mathbf{z}) \neq q(\mathbf{y} | \mathbf{z})\}, \quad (17)$$

which can be seen as more practical versions of the original  $\mathcal{Z}_1$  and  $\mathcal{Z}_2$ . Furthermore, we can prove that  $\mathcal{Z}'_2$ , which can be subsequently partitioned into  $\mathcal{S}'$  and  $\mathcal{T}'$ , is a subset of  $\mathcal{U}$  (see Proposition 2). Now we estimate diversity and correlation shift as defined in (4) and (5) by replacing  $\mathcal{S}$  and  $\mathcal{T}$  with

$$\mathcal{S}' = \{\mathbf{z} \in \mathcal{Z}'_2 \mid p(\mathbf{z}) \cdot q(\mathbf{z}) = 0\} \quad \text{and} \quad \mathcal{T}' = \{\mathbf{z} \in \mathcal{Z}'_2 \mid p(\mathbf{z}) \cdot q(\mathbf{z}) \neq 0\}, \quad (18)$$

which then give us the estimators

$$d'_{\text{div}}(p, q) = \frac{1}{2} \int_{\mathcal{S}'} |p(\mathbf{z}) - q(\mathbf{z})| d^m \mathbf{z}, \quad (19)$$

$$d'_{\text{cor}}(p, q) = \frac{1}{2} \int_{\mathcal{T}'} \sqrt{p(\mathbf{z})q(\mathbf{z})} \sum_{\mathbf{y} \in \mathcal{Y}} |p(\mathbf{y} | \mathbf{z}) - q(\mathbf{y} | \mathbf{z})| d^m \mathbf{z}. \quad (20)$$

Finally, we show (see Proposition 3 and 4) that

$$\int_{\mathcal{S}'} |p(\mathbf{z}) - q(\mathbf{z})| d^m \mathbf{z} = \int_{\mathcal{S}^*} |p(\mathbf{z}) - q(\mathbf{z})| d^m \mathbf{z}, \quad (21)$$

$$\int_{\mathcal{T}'} \sqrt{p(\mathbf{z})q(\mathbf{z})} \sum_{\mathbf{y} \in \mathcal{Y}} |p(\mathbf{y} | \mathbf{z}) - q(\mathbf{y} | \mathbf{z})| d^m \mathbf{z} = \int_{\mathcal{T}^*} \sqrt{p(\mathbf{z})q(\mathbf{z})} \sum_{\mathbf{y} \in \mathcal{Y}} |p(\mathbf{y} | \mathbf{z}) - q(\mathbf{y} | \mathbf{z})| d^m \mathbf{z}, \quad (22)$$

where

$$\mathcal{S}^* = \{\mathbf{z} \in \mathcal{U} \mid p(\mathbf{z}) \cdot q(\mathbf{z}) = 0\} \quad \text{and} \quad \mathcal{T}^* = \{\mathbf{z} \in \mathcal{U} \mid p(\mathbf{z}) \cdot q(\mathbf{z}) \neq 0\}. \quad (23)$$

The crucial difference between (18) and (23) is that  $\mathcal{S}^*$  and  $\mathcal{T}^*$  are not necessarily the subsets of  $\mathcal{Z}'_2$ , so we can compute the integrals more easily over  $\mathcal{U}$  (the output set of  $g_\phi$ ), bypassing  $\mathcal{Z}'_2$ . Once  $g_\phi$  is trained properly, inputs from training and test environments are all processed by  $g_\phi$ . Then the output features are gathered into sets  $\mathcal{Z}_{\text{tr}}$  and  $\mathcal{Z}_{\text{te}}$ , which are used for computing the shifts as in Algorithm 2 and 3 below. The preprocessing steps in line 1-5 is the same for both algorithms.

---

### Algorithm 2 Estimation of diversity shift

---

**Require:** Features  $\mathcal{Z}_{\text{tr}}$  and  $\mathcal{Z}_{\text{te}}$  from training and test environments; importance sampling size  $M$ ; threshold  $\epsilon_{\text{div}}$ .

**Ensure:** Estimated diversity shift  $d'_{\text{div}}$ .

- 1:  $\mathcal{U} \leftarrow \mathcal{Z}_{\text{tr}} \cup \mathcal{Z}_{\text{te}}$ ;
  - 2:  $\mathcal{U} \leftarrow \mathcal{U}$  scaled to zero mean and unit variance (in every dimension);
  - 3: fit distribution  $P(\mathcal{U})$  with probability function  $f$  by KDE, which induces  $P_f(\mathcal{U})$ ;
  - 4:  $(\mathcal{Z}_{\text{tr}}, \mathcal{Z}_{\text{te}}) \leftarrow$  split  $\mathcal{U}$  to recover the original partition;
  - 5: fit distributions  $P(\mathcal{Z}_{\text{tr}})$  and  $P(\mathcal{Z}_{\text{te}})$  with probability functions  $p$  and  $q$  by KDE;
  - 6:  $d'_{\text{div}} \leftarrow 0$ ;
  - 7: **for**  $t \leftarrow 1, \dots, M$  **do**
  - 8:     sample  $\mathbf{z}$  from  $P_f(\mathcal{U})$ ; ▷ sampling by importance
  - 9:     **if**  $p(\mathbf{z}) < \epsilon_{\text{div}}$  **or**  $q(\mathbf{z}) < \epsilon_{\text{div}}$  **then** ▷ check if the feature belongs to  $\mathcal{S}^*$
  - 10:          $d'_{\text{div}} \leftarrow d'_{\text{div}} + |p(\mathbf{z}) - q(\mathbf{z})|/f(\mathbf{z})$ ;
  - 11:  $d'_{\text{div}} \leftarrow d'_{\text{div}}/2M$ .
- 

### Algorithm 3 Estimation of correlation shift

---

**Require:** Features  $\mathcal{Z}_{\text{tr}}$  and  $\mathcal{Z}_{\text{te}}$  from training and test environments; importance sampling size  $M$ ; threshold  $\epsilon_{\text{cor}}$ .

**Ensure:** Estimated correlation shift  $d'_{\text{cor}}$ .

- 1:  $\mathcal{U} \leftarrow \mathcal{Z}_{\text{tr}} \cup \mathcal{Z}_{\text{te}}$ ;
  - 2:  $\mathcal{U} \leftarrow \mathcal{U}$  scaled to zero mean and unit variance (in every dimension);
  - 3: fit distribution  $P(\mathcal{U})$  with probability function  $f$  by KDE, which induces  $P_f(\mathcal{U})$ ;
  - 4:  $(\mathcal{Z}_{\text{tr}}, \mathcal{Z}_{\text{te}}) \leftarrow$  split  $\mathcal{U}$  to recover the original partition;
  - 5: fit distributions  $P(\mathcal{Z}_{\text{tr}})$  and  $P(\mathcal{Z}_{\text{te}})$  with probability functions  $p$  and  $q$  by KDE;
  - 6:  $d'_{\text{cor}} \leftarrow 0$ ;
  - 7: **for each**  $\mathbf{y} \in \mathcal{Y}$  **do**
  - 8:      $(\mathcal{Z}'_{\text{tr}}, \mathcal{Z}'_{\text{te}}) \leftarrow$  subsets of  $\mathcal{Z}_{\text{tr}}$  and  $\mathcal{Z}_{\text{te}}$  where features are extracted from the inputs with label  $\mathbf{y}$ ;
  - 9:     fit distributions  $P(\mathcal{Z}'_{\text{tr}})$  and  $P(\mathcal{Z}'_{\text{te}})$  with probability functions  $p'$  and  $q'$  by KDE;
  - 10:     **for**  $t \leftarrow 1, \dots, M$  **do**
  - 11:         sample  $\mathbf{z}$  from  $P_f(\mathcal{U})$ ; ▷ sampling by importance
  - 12:         **if**  $p(\mathbf{z}) > \epsilon_{\text{cor}}$  **and**  $q(\mathbf{z}) > \epsilon_{\text{cor}}$  **then** ▷ check if the feature belongs to  $\mathcal{T}^*$
  - 13:              $d'_{\text{cor}} \leftarrow d'_{\text{cor}} + |p'(\mathbf{z})\sqrt{q(\mathbf{z})/p(\mathbf{z})} - q'(\mathbf{z})\sqrt{p(\mathbf{z})/q(\mathbf{z})}|/f(\mathbf{z})$ ;
  - 14:  $d'_{\text{cor}} \leftarrow d'_{\text{cor}}/2M|\mathcal{Y}|$ .
-

The absolute difference in line 13 of Algorithm 3 can be derived from (20) as follows:

$$\begin{aligned}
 d'_{\text{cor}}(p, q) &= \frac{1}{2} \int_{\mathcal{T}'} \sqrt{p(\mathbf{z})q(\mathbf{z})} \sum_{\mathbf{y} \in \mathcal{Y}} |p(\mathbf{y} | \mathbf{z}) - q(\mathbf{y} | \mathbf{z})| d^n \mathbf{z} \\
 &= \frac{1}{2} \int_{\mathcal{T}'} \sum_{\mathbf{y} \in \mathcal{Y}} \left| p(\mathbf{y}, \mathbf{z}) \sqrt{q(\mathbf{z})/p(\mathbf{z})} - q(\mathbf{y}, \mathbf{z}) \sqrt{p(\mathbf{z})/q(\mathbf{z})} \right| d^n \mathbf{z} \\
 &= \frac{1}{2} \int_{\mathcal{T}'} \sum_{\mathbf{y} \in \mathcal{Y}} \left| p(\mathbf{z} | \mathbf{y}) p(\mathbf{y}) \sqrt{q(\mathbf{z})/p(\mathbf{z})} - q(\mathbf{z} | \mathbf{y}) q(\mathbf{y}) \sqrt{p(\mathbf{z})/q(\mathbf{z})} \right| d^n \mathbf{z} \quad (24) \\
 &= \frac{1}{2} \int_{\mathcal{T}'} \sum_{\mathbf{y} \in \mathcal{Y}} p(\mathbf{y}) \left| p(\mathbf{z} | \mathbf{y}) \sqrt{q(\mathbf{z})/p(\mathbf{z})} - q(\mathbf{z} | \mathbf{y}) \sqrt{p(\mathbf{z})/q(\mathbf{z})} \right| d^n \mathbf{z} \\
 &= \frac{1}{2} \sum_{\mathbf{y} \in \mathcal{Y}} p(\mathbf{y}) \int_{\mathcal{T}'} \left| p(\mathbf{z} | \mathbf{y}) \sqrt{q(\mathbf{z})/p(\mathbf{z})} - q(\mathbf{z} | \mathbf{y}) \sqrt{p(\mathbf{z})/q(\mathbf{z})} \right| d^n \mathbf{z}.
 \end{aligned}$$

## B.2 Implementation details

Same as the networks on which the algorithms in Section 3.1 are trained, we use MLP for Colored MNIST and ResNet-18 for other datasets as the feature extractors. All ResNet-18 models are pretrained on ImageNet except for NICO. The feature extractors are optimized by Adam with fixed learning rate 0.0003 for  $T = 2000$  iterations. The batch size  $N$  we used is 32 for each environment, and we set the feature dimension  $m = 8$ . For every random data split, we keep 80% data for training and use the rest 20% data for validation. We choose the models maximizing the accuracy (in predicting the environments) on validation sets. As for Algorithm 2 and 3, the importance sampling size  $M = 10000$ , and we empirically set the thresholds  $\epsilon_{\text{div}} = 1 \times 10^{-12}$  and  $\epsilon_{\text{cor}} = 5 \times 10^{-4}$ . We use Gaussian kernels for all the KDEs.

## C Estimation Results with Error Bars

The table below lists all the results that have been plotted in Figure 3 with standard error bars. The statistics are averaged over five runs of different weight initializations and training/validation splits.

Table 4: Estimation of diversity and correlation shift.

| Dataset         | Div. shift  | Cor. shift  |
|-----------------|-------------|-------------|
| i.i.d. data     | 0.00 ± 0.00 | 0.00 ± 0.00 |
| PACS            | 0.82 ± 0.05 | 0.00 ± 0.00 |
| Office-Home     | 0.17 ± 0.02 | 0.04 ± 0.02 |
| Terra Incognita | 0.98 ± 0.04 | 0.00 ± 0.00 |
| Camelyon        | 0.98 ± 0.02 | 0.00 ± 0.00 |
| DomainNet       | 0.11 ± 0.02 | 0.33 ± 0.03 |
| Colored MNIST   | 0.00 ± 0.00 | 0.62 ± 0.04 |
| CelebA          | 0.04 ± 0.01 | 0.17 ± 0.04 |
| NICO            | 0.00 ± 0.00 | 0.53 ± 0.04 |
| ImageNet-A      | 0.02 ± 0.00 | 0.04 ± 0.01 |
| ImageNet-R      | 0.04 ± 0.01 | 0.08 ± 0.02 |
| ImageNet-V2     | 0.01 ± 0.00 | 0.13 ± 0.03 |
| ImageNet-Sketch | 0.45 ± 0.02 | 0.01 ± 0.01 |

## D Datasets

- **PACS** [39] comprises four domains  $d \in \{\text{photos, art, cartoons, sketches}\}$ . This dataset contains 9,991 examples of dimension (3, 224, 224) and 7 classes.
- **OfficeHome** [69] includes domains  $d \in \{\text{art, clipart, product, real}\}$ . This dataset contains 15,588 examples of dimension (3, 224, 224) and 65 classes.
- **Terra Incognita** [12] contains photographs of wild animals taken by camera traps at locations  $d \in \{\text{L100, L38, L43, L46}\}$ . Following DomainBed [27], our version of this dataset contains 24,788 examples of dimension (3, 224, 224) and 10 classes.

- **WILDS-Camelyon17** [35] is a patch-based variant of the Camelyon17 dataset [16] curated by WILDS [35]. This dataset contains 455,954 examples of dimension (3, 224, 224) and 2 classes collected and processed by 5 hospitals.
- **Colored MNIST** [7] is a variant of the MNIST handwritten digit classification dataset [38]. Following IRM [7], this dataset contains 60,000 examples of dimension (2, 14, 14) and 2 classes.
- **NICO** [29] consists of real-world photos of animals and vehicles captured in a wide range of context. There are 9 or 10 different contexts for each class of animal and vehicle. Our version make use of both classes appeared in four overlapped contexts: “on snow”, “in forest”, “on beach” and “on grass” to construct training and test environments (as in Table 5) that are similar to the setting of Colored MNIST. In total, our split consists of 4,080 examples of dimension (3, 224, 224) and 2 classes.

Table 5: Environment splits of NICO and the number of examples in each group.

| Environment | Class   | on snow | in forest | on beach | on grass |
|-------------|---------|---------|-----------|----------|----------|
| Training 1  | Animal  | 10      | 400       | 10       | 400      |
|             | Vehicle | 400     | 10        | 400      | 10       |
| Training 2  | Animal  | 20      | 390       | 20       | 390      |
|             | Vehicle | 390     | 20        | 390      | 20       |
| Validation  | Animal  | 50      | 50        | 50       | 50       |
|             | Vehicle | 50      | 50        | 50       | 50       |
| Test        | Animal  | 90      | 10        | 90       | 10       |
|             | Vehicle | 10      | 90        | 10       | 90       |

- **CelebA** [45] is a large-scale face attributes dataset with more than 200K celebrity images, each with 40 attribute annotations. Our version uses a subset of 27,040 images divided into three environments, simulating the setting of Colored MNIST (where there is large correlation shift). We make full use of the group (blond-hair males) that has the least number of images. See Table 6 for more details regarding the environment splits.

Table 6: Environment splits of CelebA and the number of examples in each group.

| Environment | Class     | Male   | Female |
|-------------|-----------|--------|--------|
| Training 1  | blond     | 462    | 11,671 |
|             | not blond | 11,671 | 462    |
| Training 2  | blond     | 924    | 11,209 |
|             | not blond | 11,209 | 924    |
| Test        | blond     | 1,387  | 1,387  |
|             | not blond | 1,387  | 1,387  |

## E Algorithms

We conduct a survey on various existing OoD generalization algorithms, and here we summarize some of their notable requirements and properties:

1. **Requires more than one training environments** — the algorithm only works on datasets with multiple training environments that follow different distributions.
2. **Requires environment labels** — the algorithm works only when the index of each training environment is accessible during training.
3. **Evaluated on datasets dominated by diversity shift** — the algorithm has been evaluated on datasets dominated by diversity shift (according to our estimation).

4. **Evaluated on datasets dominated by correlation shift** — the algorithm has been evaluated on datasets dominated by correlation shift (according to our estimation).
5. **Uses test set for model selection** — the performance of the algorithm (on some datasets) is evaluated on the models selected by test-domain validation.
6. **Only works on image data** — the main techniques of the algorithm involves operations on images, which do not work on other kinds of data.

Table 7: Properties of OoD generalization algorithms.

| Algorithm   | Property 1 | Property 2 | Property 3 | Property 4 | Property 5    | Property 6 |
|-------------|------------|------------|------------|------------|---------------|------------|
| ERM         | False      | False      | False      | False      | False         | False      |
| IRM         | True       | False      | False      | True       | True          | False      |
| GroupDRO    | False      | False      | N/A        | True       | False         | False      |
| Mixup       | True       | True       | N/A        | N/A        | Not specified | False      |
| MLDG        | True       | False      | True       | False      | Not specified | False      |
| CORAL       | False      | False      | True       | False      | True          | False      |
| MMD         | True       | False      | N/A        | N/A        | Not specified | False      |
| DANN        | True       | True       | N/A        | N/A        | Not specified | False      |
| MTL         | True       | True       | N/A        | N/A        | Not specified | False      |
| SagNet      | False      | False      | True       | False      | Not specified | False      |
| ARM         | False      | False      | N/A        | N/A        | Not specified | False      |
| VREx        | True       | False      | True       | True       | True          | False      |
| RSC         | False      | False      | True       | False      | False         | False      |
| ANDMask     | True       | False      | N/A        | N/A        | Not specified | False      |
| IGA         | True       | False      | False      | True       | Not specified | False      |
| ERDG [79]   | True       | True       | True       | True       | False         | False      |
| SD [55]     | False      | False      | False      | True       | True          | False      |
| TTT [65]    | False      | False      | True       | False      | False         | True       |
| JiGen [17]  | False      | False      | True       | False      | False         | True       |
| DecAug [10] | True       | True       | True       | True       | True          | False      |

## F Model Selection Methods

Among the three model selection methods we used, *training-domain validation* and *test-domain validation* are concisely described in [27]. Here we quote:

**Training-domain validation** We split each training domain into training and validation subsets. We train models using the training subsets, and choose the model maximizing the accuracy on the union of validation subsets. This strategy assumes that the training and test examples follow similar distribution.

**Test-domain validation** We choose the model maximizing the accuracy on a validation set that follows the distribution of the test domain. We allow one query (the last checkpoint) per choice of hyperparameters, disallowing early stopping.

Besides, we use *OoD validation* in place of *leave-one-domain-out validation* (another method employed in [27]) out of two considerations: (i) the Camelyon dataset is an official benchmark listed in WILDS [35], which inherently comes with an OoD validation set and the corresponding selection method is mandatory for participating in the benchmark; (ii) given  $k$  training domains, leave-one-domain-out validation is computationally costly (especially when  $k$  is large), increasing the number of experiments by  $k - 1$  times. Moreover, when  $k$  is small (e.g.  $k = 2$  in Colored MNIST), the method heavily reduces the number of training examples accessible to the models. OoD validation can be seen as a simplification of the leave-one-domain-out validation method.

**OoD validation** We choose the model maximizing the accuracy on a validation set that follows *neither* the distribution of the training domain or the distribution of the test domain. This strategy assumes that the models generalizing well on the OoD validation set also generalize well on the test set.

## G Hyperparameter Search Space

For convenient comparison, we have followed the search space proposed in [27] whenever possible.

Table 8: Hyperparameters, their default values and distributions for random search.

| Condition | Hyperparameter                     | Default value | Random distribution               |
|-----------|------------------------------------|---------------|-----------------------------------|
| ResNet    | learning rate                      | 0.00005       | $10^{\text{Uniform}(-5, -3.5)}$   |
|           | batch size                         | 32            | $2^{\text{Uniform}(3, 5.5)}$      |
|           | batch size (if CelebA)             | 48            | $2^{\text{Uniform}(4.5, 6)}$      |
|           | batch size (if ARM)                | 8             | 8                                 |
|           | ResNet dropout                     | 0             | 0                                 |
|           | generator learning rate            | 0.00005       | $10^{\text{Uniform}(-5, -3.5)}$   |
|           | discriminator learning rate        | 0.00005       | $10^{\text{Uniform}(-5, -3.5)}$   |
|           | weight decay                       | 0             | $10^{\text{Uniform}(-6, -2)}$     |
|           | generator weight decay             | 0             | $10^{\text{Uniform}(-6, -2)}$     |
| MLP       | learning rate                      | 0.001         | $10^{\text{Uniform}(-4.5, -3.5)}$ |
|           | batch size                         | 64            | $2^{\text{Uniform}(3, 9)}$        |
|           | generator learning rate            | 0.001         | $10^{\text{Uniform}(-4.5, -2.5)}$ |
|           | discriminator learning rate        | 0.001         | $10^{\text{Uniform}(-4.5, -2.5)}$ |
|           | weight decay                       | 0             | 0                                 |
|           | generator weight decay             | 0             | 0                                 |
| IRM       | lambda                             | 100           | $10^{\text{Uniform}(-1, 5)}$      |
|           | iterations annealing               | 500           | $10^{\text{Uniform}(0, 4)}$       |
|           | iterations annealing (if CelebA)   | 500           | $10^{\text{Uniform}(0, 3.5)}$     |
| VREx      | lambda                             | 10            | $10^{\text{Uniform}(-1, 5)}$      |
|           | iterations annealing               | 500           | $10^{\text{Uniform}(0, 4)}$       |
|           | iterations annealing (if CelebA)   | 500           | $10^{\text{Uniform}(0, 3.5)}$     |
| Mixup     | alpha                              | 0.2           | $10^{\text{Uniform}(0, 4)}$       |
| GroupDRO  | eta                                | 0.01          | $10^{\text{Uniform}(-1, 1)}$      |
| MMD       | gamma                              | 1             | $10^{\text{Uniform}(-1, 1)}$      |
| CORAL     | gamma                              | 1             | $10^{\text{Uniform}(-1, 1)}$      |
| MTL       | ema                                | 0.99          | RandomChoice([0.5, 0.9, 0.99, 1]) |
| DANN      | lambda                             | 1.0           | $10^{\text{Uniform}(-2, 2)}$      |
|           | disc weight decay                  | 0             | $10^{\text{Uniform}(-6, 2)}$      |
|           | discriminator steps                | 1             | $2^{\text{Uniform}(0, 3)}$        |
|           | gradient penalty                   | 0             | $10^{\text{Uniform}(-2, 1)}$      |
|           | Adam $\beta_1$                     | 0.5           | RandomChoice([0, 0.5])            |
| MLDG      | beta                               | 1             | $10^{\text{Uniform}(-1, 1)}$      |
| RSC       | feature drop percentage            | 1/3           | Uniform(0, 0.5)                   |
|           | batch drop percentage              | 1/3           | Uniform(0, 0.5)                   |
| SagNet    | adversary weight                   | 0.1           | $10^{\text{Uniform}(-2, 1)}$      |
| ANDMask   | tau                                | 1             | Uniform(0.5, 1.0)                 |
| IGA       | penalty                            | 1,000         | $10^{\text{Uniform}(1, 5)}$       |
| ERDG      | discriminator learning rate        | 0.00005       | $10^{\text{Uniform}(-5, -3.5)}$   |
|           | $T'$ learning rate                 | 0.000005      | $10^{\text{Uniform}(-6, -4.5)}$   |
|           | $T$ learning rate                  | 0.000005      | $10^{\text{Uniform}(-6, -4.5)}$   |
|           | adversarial loss weight            | 0.5           | $10^{\text{Uniform}(-2, 0)}$      |
|           | entropy regularization loss weight | 0.01          | $10^{\text{Uniform}(-4, -1)}$     |
|           | cross-entropy loss weight          | 0.05          | $10^{\text{Uniform}(-3, -1)}$     |